International Journal of Microwave and Wireless Technologies

cambridge.org/mrf

A broadband metasurface antenna with multimode resonance

Hui Pang, Jianping Zhao and Juan Xu

Cyberspace Security Academy, Qufu Normal University, Qufu, China

Research Paper

Cite this article: Pang H, Zhao J, Xu J (2024) A broadband metasurface antenna with multimode resonance. *International Journal of Microwave and Wireless Technologies*, 1–8. https://doi.org/10.1017/S1759078724000588

Received: 25 April 2023
Revised: 6 May 2024
Accepted: 15 May 2024

Keywords:
broadband; characteristic mode theory; metasurface; multimode resonance

Corresponding author: Juan Xu;
Email: xujuan125@163.com

Abstract

A multiresonance metasurface antenna is proposed which has wide bandwidth and low-profile. The characteristic mode theory is used to design antenna structure. Three ideal modes are obtained by adjusting the mode currents to optimize the radiation performance of the antenna. The characteristic mode analysis is used to model, analyze, and optimize the antenna, revealing the physical characteristics of the metasurface antenna. The slot is not only used as the feeding structure for exciting characteristic modes but also introduces a slot mode. Combining the slot mode with the metasurface modes, the bandwidth of the antenna is broadened. The antenna element has a relative bandwidth of 43.7%. To obtain higher gain, a 2×2 antenna array is proposed. The antenna array is simulated, fabricated, and measured. The results show that the relative bandwidth of the proposed metasurface antenna array is 31.6% with the gain of 12.3–15.8 dBi over the operating bandwidth.

Introduction

With the development of wireless communication systems, the demand for microstrip antennas is increasing [1]. Microstrip patch antenna has been widely used in many applications due to its advantages of low cost, small shape, and light weight. However, microstrip antenna often has the disadvantage of narrow bandwidth, how to make the antenna work in a wider bandwidth has become the current research hotspot.

The main traditional methods to broaden the bandwidth of microstrip antennas are [2]: (1) improve the feeding structure, such as electromagnetic coupling feed, L-shaped probe, or M-shaped probe, but this leads to a high cross-polarization. (2) Use high thickness or low dielectric constant dielectric substrate to reduce the equivalent circuit Q value, but this will lead to poor radiation efficiency of the antenna. (3) Use parasitic elements to couple multiple resonant modes to increase the bandwidth, but this will increase the size of the antenna.

Recently, to improve the performance of antennas, metamaterials have attracted great interest from researchers due to their unique properties. As a metamaterial, the metasurface is used in antennas [3–8]. In Ref. [9], the metasurface is angled to obtain the circularly polarized characteristic. In Ref. [10], an omnidirectional radiating metasurface antenna is proposed, and a bandwidth of 31% is obtained with an average antenna gain of 6.34 dBi. In Ref. [11], a wideband grid slot patch antenna based on metamaterial is proposed. When |S11| is less than −10 dB, the measured bandwidth is 28% and the maximum gain is 9.8 dBi. Ref. [12] further points out that when there are multiple metasurface microstrip antennas, the mutual coupling between them will excite their respective higher order modes (HOMs), and the radiation of these (HOMs) will cause the pattern to split. However, to obtain the bandwidth performance, further research is still needed. The metasurface antenna proposed in Ref. [13], the characteristic mode theory (CMT) is used to analyze the metasurface antenna, and the antenna structure obtained a relative bandwidth of 30% and an average gain of 7.28 dBi.

In this paper, the antenna structure is guided and optimized using CMT. The process achieves a physical interpretation of the antenna operation mechanism. The mode properties of the metasurface were analyzed. Three modes are excited through the slot and the slot inspires a resonance frequency. The three modes are combined with the slot mode to obtain a multimode broadband antenna.

Configuration and operating concepts

Geometry of the antenna

The overall geometry of the proposed metasurface antenna is shown in Fig. 1. The proposed structure consists of two substrate layers and three mental layers. The dielectric substrate of Rogers RO4003C ($\varepsilon_r = 3.55$, $\tan\delta = 0.002$) is used throughout and the thicknesses are 3.2 mm and 0.813 mm. The metasurface patch consists of a nonuniform array of rectangular patches.

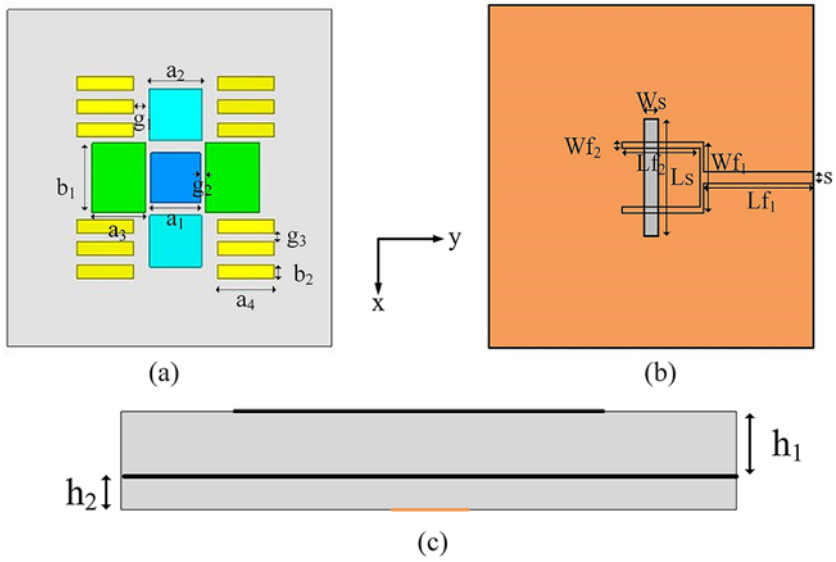

Figure 1. Geometry of proposed metasurface antenna. (a) Top view, (b) bottom view, and (c) side view.

Table 1. Detailed dimensions of the proposed antenna unit (mm)

a_1	a_2	a_3	a_4	b_1	b_2	g_1	g_2	g_3	Lf_2	s
7.4	7.7	8	8.45	10.4	2	3.4	1.9	2.35	12.75	1.7
h_1	h_2	Wf_1	Wf_2	Ws	Ls	Lf_1				
3.2	0.813	10.4	0.9	2.4	17.2	16.4				

A square patch is placed in the center, two square patches of the same size are placed on the left and right sides of the center patch, and two rectangular patches of the same size are placed above and below the center. Four rectangular patches are placed at the corners, three rectangular slots etched above them. The ground plane is between two dielectric substrates, and a rectangular slot is etched in the middle. The bottom layer is a Y-shaped feeding structure. The parameters of the proposed antenna are shown in Table 1.

Operating mechanism

To obtain the patch size of Fig. 4(a), we use some formulas to calculate [14]. For a rectangular microstrip antenna with operating frequency f, the width W of the radiation patch can be estimated. It can also be estimated the equivalent radiation slot length Ws through the formula in Ref. [14]. Figure 3(b) calculates the model significance (MS) through the formula [1]. By using the above formula, the initial patch size w and slot size Ws of the metasurface antenna can be obtained. To better demonstrate the design principle of the proposed antenna size, Fig. 2 shows the simulated S11 of a 3 × 3 traditional metasurface antenna at different sizes. It can be seen that the calculated parameter w achieves the best impedance matching and has a wide bandwidth. The length of Ws has less effect on S11. Based on this, we continue to improve the design to obtain the antenna structure shown. Assemble the obtained antenna structure into an array and fabricate the antenna array. The reflection property of the square patch unit is analyzed using the Floquet-port HFSS model. Figure 3 shows that W and unit spacing g have a significant impact on the reflection property. The zero reflection phase point will be affected by changes in w and g. Thus square patches with different sizes are formed into a nonuniform metasurface structure. As a result, multiple resonant modes can be excited together with the resonant mode of the coupling slot to obtain broadband performance.

The result is obtained using the MoM-based characteristic mode analysis (CMA) tool in commercial simulation software CST. It can be seen from the MS that mode 1/2, mode 7/8 and mode 9/10 are three pairs of degenerate modes. For degenerate mode, only y-polarized mode currents are given. Observing the radiation patterns in Fig. 5(a), it can be observed that mode 2 has lateral radiation, and mode 3, mode 4, mode 5, and mode 6 exhibit a

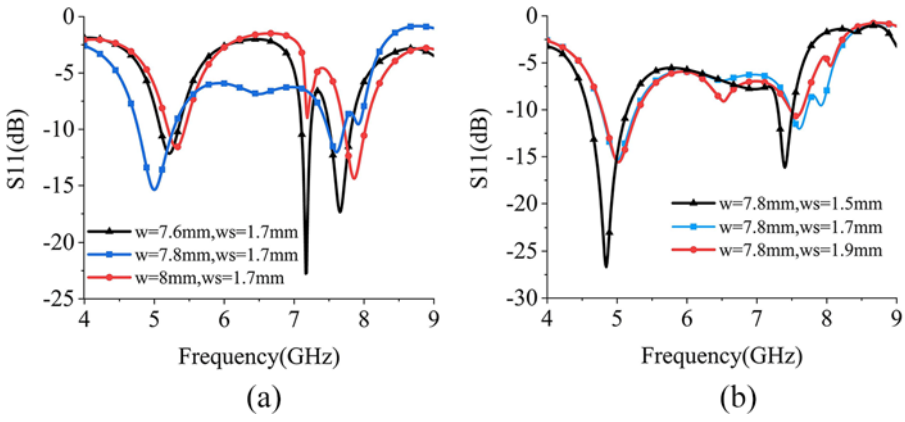

Figure 2. Simulated S11 of 3 × 3 traditional metasurface antenna at different sizes, (a) different lengths of w and (b) different lengths of Ws.

https://doi.org/10.1017/S1759078724000588 Published online by Cambridge University Press

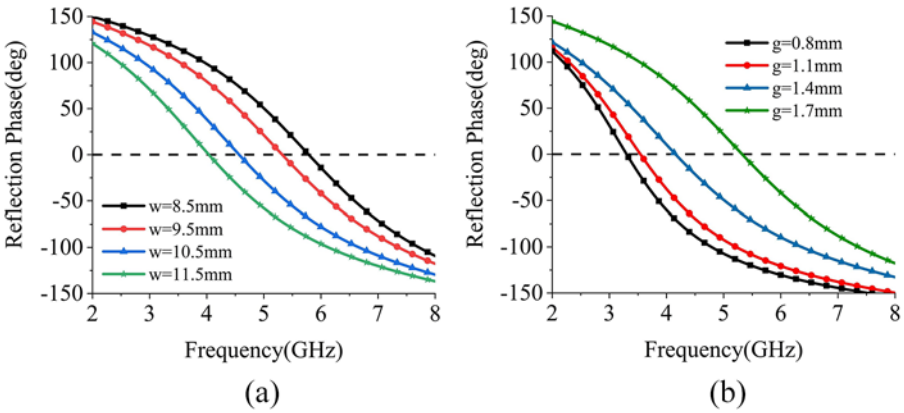

Figure 3. Reflection phase at different sizes, (a) different lengths of *w* and (b) different lengths of *g*.

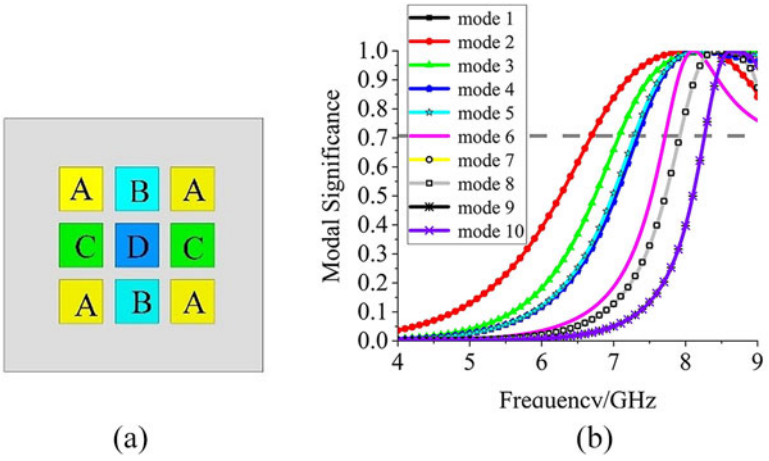

Figure 4. (a) Configuration of the traditional metasurface and (b) modal significance of the traditional metasurface.

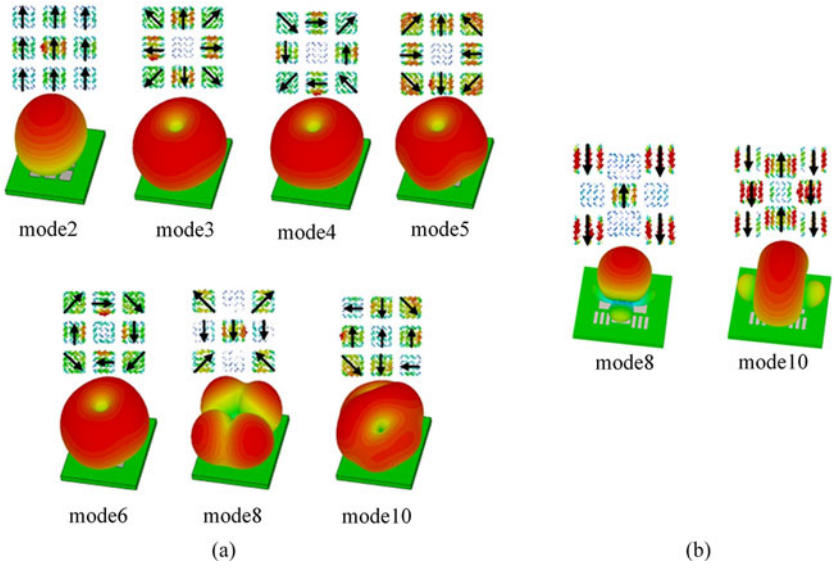

Figure 5. Model currents and radiation patterns of the modes. (a) Radiation patterns and model currents of the traditional metasurface and (b) radiation patterns and model currents of the optimized metasurface.

omnidirectional radiation, and the current distribution is disordered, so they are not considered. The mode 8 pattern is split, and the mode 10 pattern has larger sidelobes. Further observation of the mode currents of each mode in Fig. 5(a) shows that the current of mode 2 is mainly concentrated on the central patch, and the current direction on the patch is *y* polarization, thus, mode 2 has good radiation directivity. Observe the surface current of mode 8, the current is mainly concentrated on the A, C, and D patches. The current directions on the C and D patches are the same. Therefore, the pattern splitting of mode 8 is caused by the inconsistent current directions on the A patches and the C and D patches. Modify the size of patch A and etch slots along the y-axis on patch A to truncate the original rectangular patch into three parts. The etched slots can successfully weaken or reverse the

https://doi.org/10.1017/S1759078724000588 Published online by Cambridge University Press

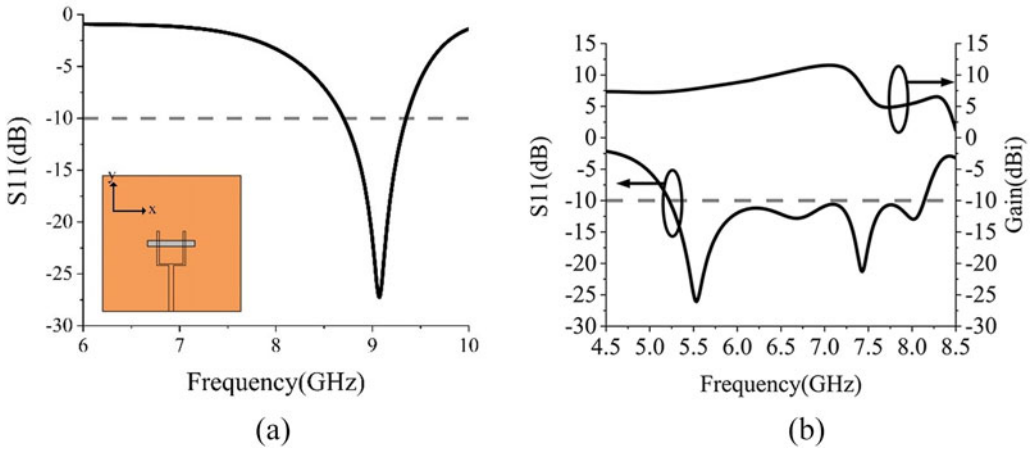

Figure 6. Simulated and surface current. (a) Simulated S11 without metasurface and (b) simulated |S11| and gain of proposed antenna.

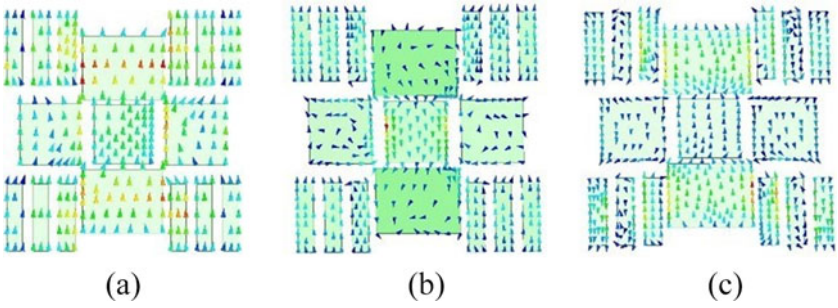

Figure 7. Simulated surface current at different frequencies. (a) 5.5 GHz, (b) 6.6 GHz, and (c) 7.4 GHz.

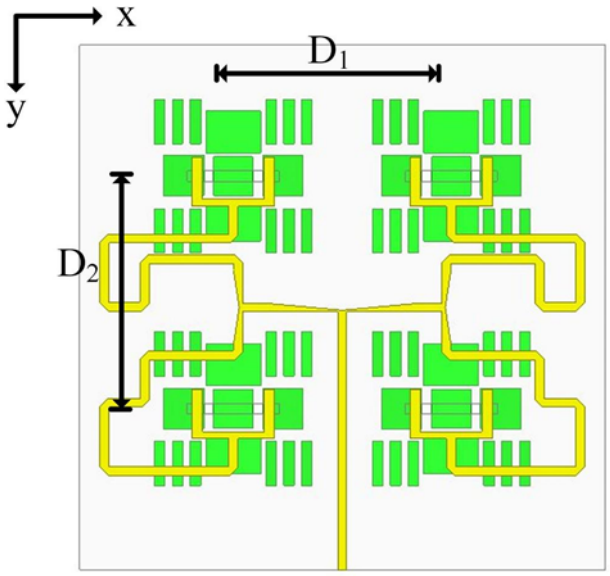

Figure 8. Configuration of the 2 × 2 antenna array.

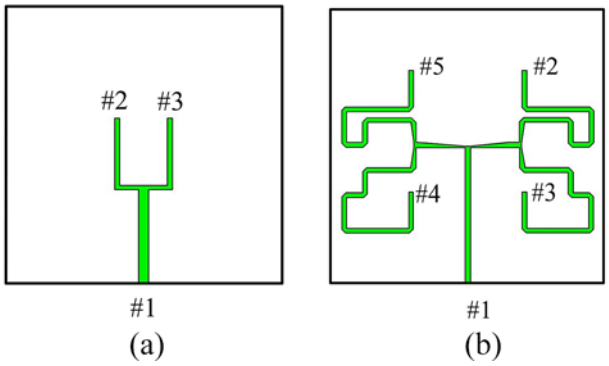

Figure 9. Power divider. (a) Two-way microstrip power divider and (b) four-way microstrip power divider.

modal currents along the *x*-axis while not decreasing the required modal currents along the *y*-axis. Observe mode 10, the surface current of patch B and patch C is opposite. Adjust the size and spacing of patch B and patch C so that the current on the patch C and patch A are in the same direction and occupy a dominant position. The metasurface structure as shown in Fig. 1(a) is finally obtained by adjusting the size through trial and error. Figure 5(b) is the pattern of optimized mode 8 and mode 9. It can be seen that the radiation directivity of the modes is good.

Selecting the appropriate feeding structure to excite the metasurface. A rectangular slot along the *x*-axis is etched on the ground, and a *y*-shaped feeding structure is used to excite the modes with a *y*-polarized current. To further prove the working mechanism, the commercial simulation software HFSS is used to simulate the metasurface antenna, and the broadband metasurface element is obtained. At the same time, the slot feeding structure without metasurface is simulated and analyzed. From Fig. 6(a), it can be seen that the resonance point at the high frequency of the metasurface element is introduced by the radiation slot, which makes

https://doi.org/10.1017/S1759078724000588 Published online by Cambridge University Press

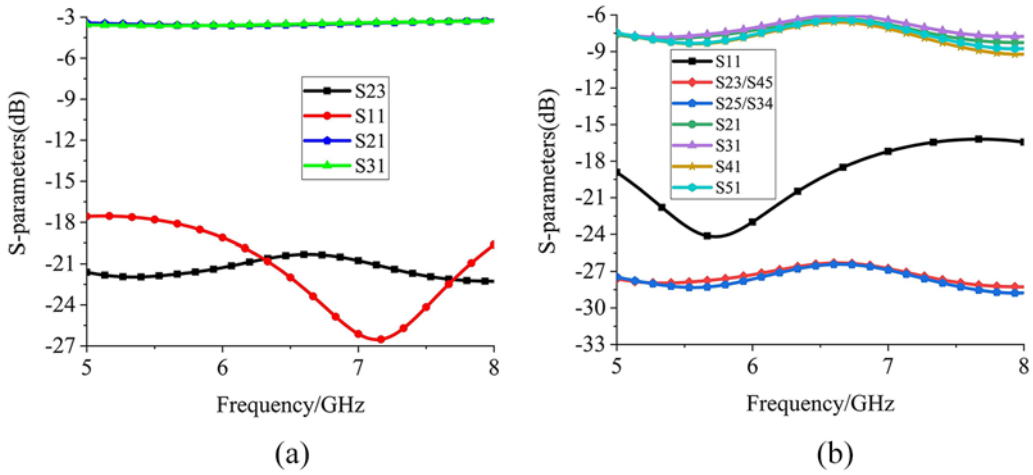

Figure 10. S-parameters of the power divider. (a) S-parameters of the two-way power divider and (b) S-parameters of the four-way power divider.

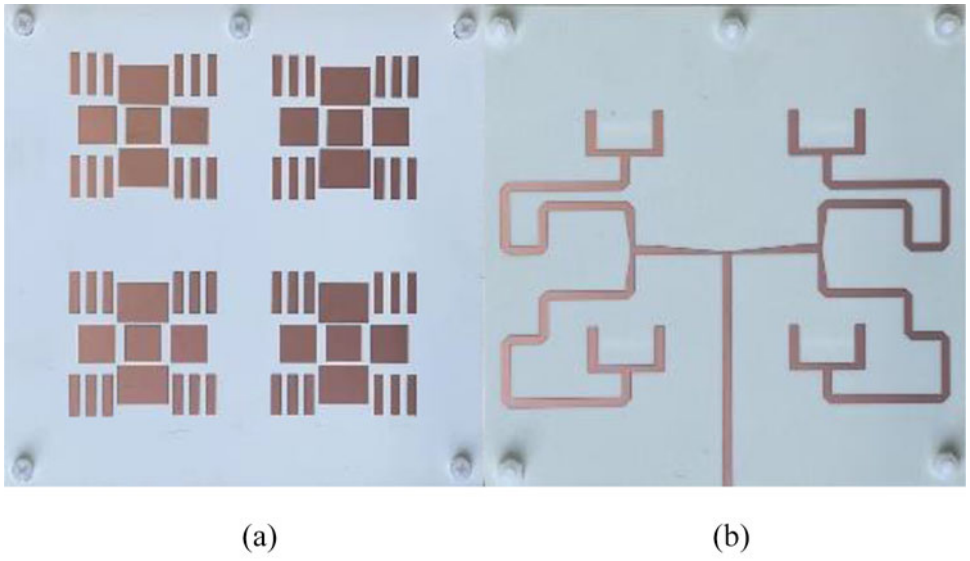

Figure 11. Photographs of the fabricated antenna. (a) Top view and (b) back view.

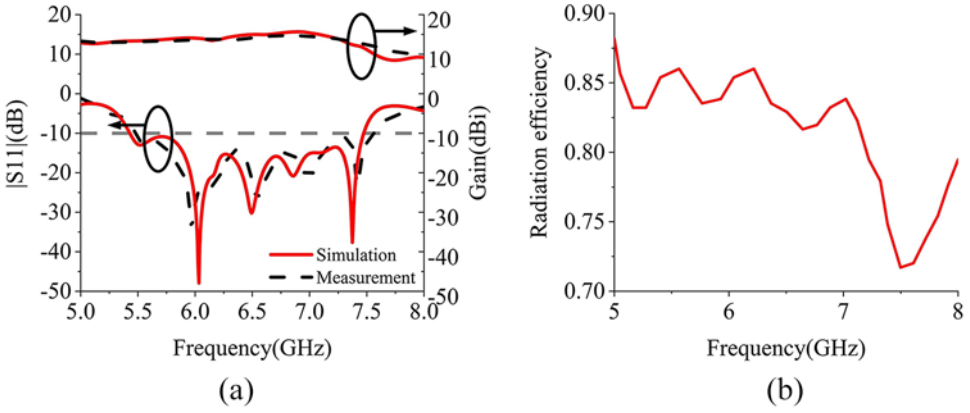

Figure 12. Simulated and measured results. (a) Simulated and measured |S11| and realized gain of the proposed antenna and (b) measured radiation efficiency of the proposed antenna.

https://doi.org/10.1017/S1759078724000588 Published online by Cambridge University Press

the antenna structure have multiple resonance points. As shown in Fig. 6(b), the relative bandwidth of the obtained metasurface unit |S11| is 43.7%, with great broadband characteristic. For further verification, Fig. 7 gives the current of three resonance points of the metasurface antenna, which corresponds to the three mode currents in Fig. 5(b).

The design of the antenna array

A 2 × 2 antenna array is designed based on the proposed metasurface antenna element. Finally, we get the arrangement method as shown in Fig. 8. To facilitate the analysis of the characteristics of the proposed power divider, the two-way microstrip power divider of Fig. 9(a) is first analyzed and its S-parameters are shown in Fig. 10(a). From Fig. 10(a) it can be seen that the S11 of the input port #1 of the antenna is lower than −15 dB. Insertion loss between output ports #2, #3 and input port #1 is −3 dB. Isolation between output ports S23 is less than −20 dB. The two-way microstrip power divider has good performance. To improve the gain of the antenna, the antenna elements are arranged into an array. Because the two-way microstrip power divider has been analyzed separately, it can be considered as an output port. Therefore the proposed power divider is approximated as a four-way microstrip power divider as shown in Fig. 9(b). Figure 10(b) shows the characteristics of the power divider in Fig. 9(b). It can be seen that the S11 of input port #1 in the antenna array instantaneous bandwidth (IBW) is lower than −15 dB, and the insertion loss of #2, #3, #4, and #5 is −6 dB. The isolation between the output port and the input port is less than −20 dB, indicating weak coupling between the output ports. The results of D1 and D2 are obtained using the commercial simulation software HFSS. The optimized $D1 = 41.5$ mm and $D2 = 44.3$ mm.

Simulation and measurement

The photograph of the fabricated antenna is shown in Fig. 11, Fig. 11(a) and (b) shows the front side and the back side of the antenna respectively. The proposed antenna is simulated and measured. In this article, the antenna was installed in a 9 m × 6 m × 6 m microwave anechoic chamber. An Agilent N5244A network analyzer was used to obtain the performance of the antenna. Figure 12(a) shows the simulated and measured |S11| and gain of the antenna array. It can be observed that the measured and simulated curves of the antenna match well and a relative bandwidth of 31.3% (5.43–7.47 GHz) is obtained, with gain peaks up to 15.8 dBi in the operating band. Figure 12(b) shows the measurement result of the radiation efficiency of the designed antenna. In addition, efficiency is also an important indicator of the antenna which can be calculated through the formula [14].

The reason for not giving the simulation curve of the efficiency is the weak radiation boundary electric field using the commercial software HFSS for simulation, the adaptive grid is not dense enough. The data dispersion error causes the received energy of the integration to be greater than the port energy. The final efficiency obtained is greater than 1. So there is a significant error in calculating the efficiency of antennas with low losses using HFSS. The measured average radiation efficiency is above 85%. The efficiency decreases at high frequency due to microstrip line loss and other reasons.

Figure 13(a–e) shows the patterns of E-plane and H-plane measurements and simulations at 5.5 GHz, 6 GHz, 6.5 GHz, 6.8 GHz, and 7.4 GHz. It can be observed that the simulated and measured radiation patterns coincide with each other. The antenna achieves stable radiation performance with nearly identical main

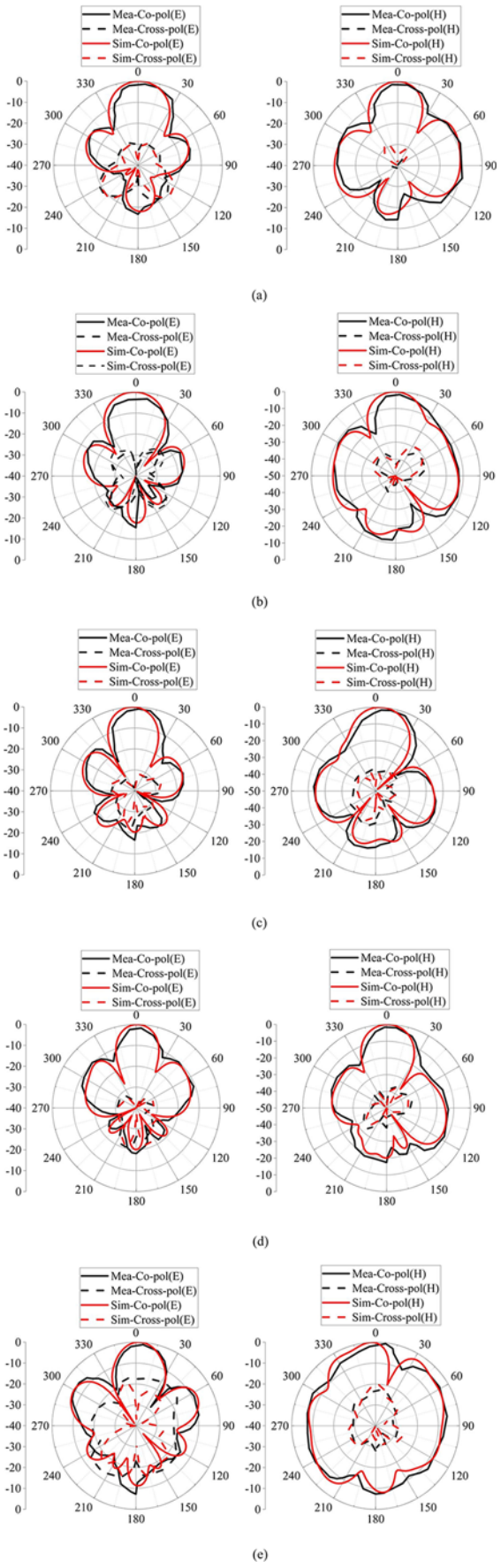

Figure 13. E-plane and H-plane radiation pattern (a) at 5.5 GHz, (b) at 6 GHz, (c) at 6.5 GHz, (d) at 6.8 GHz, and (e) at 7.4 GHz.

https://doi.org/10.1017/S1759078724000588 Published online by Cambridge University Press

Table 2. Performance comparison with the proposed antenna

Ref.	Size (λ^2)	Height (λ)	f_0 (GHz)	Impedance bandwidth	Peak gain (dB)	Feedingstructure
3	0.88 × 0.88	0.05	3.25	36%	8.9	Microstrip
8	1.0 × 1.0	0.07	5.5	28.2%	5.8	Microstrip
15	0.58 × 0.58	0.07	5.25	36.3%	6.05	Microstrip
16	1.0 × 1.0	0.058	6	25.08	8	Coplanar waveguide
17	1.15 × 1.15	0.1	7	37.7%	8.7	Microstrip and coaxial
18	0.91 × 0.91	0.07	5.5	26.73%	8.54	Coplanar waveguide
19	2.42 × 2.42	0.06	6	32.62%	7.2	Coaxial
Element	0.75 × 0.75	0.06	6.5	43.7%	10.6	Microstrip
Array	1.6 × 1.6	0.06	6.5	31.6%	15.8	Microstrip power divider

polarization gain directional in the E-plane and H-plane and with little variation in beamwidth within the band. There is a split at 7.4 GHz, which is because the slot pattern does not provide good broadside radiation. This also causes a slight decrease in the gain of the antenna at high frequency.

Table 2 shows the comparison of the proposed antenna and other antennas reported in the literatures. Obviously, the bandwidth of the proposed structure is the widest. The low profile of Ref. [3] is at the expense of antenna gain. The antenna element proposed in this paper uses a Y-shaped microstrip line feeding structure, and on this basis, a microstrip power divider is designed to successfully form an antenna array. The antenna array not only has a wide bandwidth, but also improves the gain.

Conclusion

In this work, a broadband low-profile linearly polarized patch antenna using metasurface has been presented, analyzed, and experimentally verified. Through the coupling slot, multiple adjacent resonant frequencies can be excited to achieve broadband operation. CMA provides a clear explanation for the broadband operation and radiation performance of the antenna structure. The obtained bandwidth of the antenna element is 5.22–8.14 GHz, and the relative bandwidth is 43.7% and the proposed antenna array achieves a 3 dB gain bandwidth of about 31.3%.

Funding. This work was supported in part by Shandong Natural Science Foundation of ZR2023MF038 and the National Natural Science Foundation of China (61701278).

Competing interests. The author declares that there is no conflict of interest regarding the publication of this paper.

References

1. **Higgins H** (2007) Body implant communication – Is it a reality? In *2007 IET Seminar on Antennas and Propagation for Body-Centric Wireless Communications*, London, 33–36.
2. **Wong KL** (2002) *Compact and Broadband Microstrip Antennas*. New York: John Wiley & Sons, Ltd.
3. **Liu S, Yang D, Chen Y, Zhang X and Xiang Y** (2021) High isolation and low cross-polarization of low-profile dual-polarized antennas via metasurface mode optimization. *IEEE Transactions on Antennas and Propagation* **69**(5), 2999–3004.
4. **Li T and Chen ZN** (2020) Wideband sidelobe-level reduced Ka-band metasurface antenna array fed by substrate-integrated gap waveguide using characteristic mode analysis. *IEEE Transactions on Antennas and Propagation* **68**(3), 1356–1365.
5. **Liu S, Yang D, Chen Y, Zhang X and Xiang Y** (2020) Compatible integration of circularly polarized omnidirectional metasurface antenna with solar cells. *IEEE Transactions on Antennas and Propagation* **68**(5), 4155–4160.
6. **Swain R, Chatterjee A, Nanda S and Mishra RK** (2020) A linear-to-circular polarization conversion metasurface based wideband aperture coupled antenna. *Journal of Electrical Engineering & Technology* **15**, 1293–1299.
7. **Yang X, Liu Y and Gong S-X** (2018) Design of a wideband omnidirectional antenna with characteristic mode analysis. *IEEE Antennas and Wireless Propagation Letters* **17**(6), 993–997.
8. **Gao X, Tian G, Shou Z and Li S** (2021) A low-profile broadband circularly polarized patch antenna based on characteristic mode analysis. *IEEE Antennas and Wireless Propagation Letters* **20**(2), 214–218.
9. **Dong J, Wu R, Yuan X and Mo J** (2022) A low-profile broadband circularly polarized metasurface antenna based on characteristic mode analysis. Waves in Random and Complex Media.
10. **Feng G, Chen L, Xue X and Shi X** (2017) Broadband surface-wave antenna with a novel nonuniform tapered metasurface. *IEEE Antennas and Wireless Propagation Letters* **16**, 2902–2905.
11. **Liu W, Chen ZN and Qing X** (2015) Metamaterial-based low-profile broadband aperture-coupled grid-slotted patch antenna. *IEEE Transactions on Antennas and Propagation* **63**(7), 3325–3329.
12. **Lin FH and Chen ZN** (2018) A method of suppressing higher order modes for improving radiation performance of metasurface multiport antennas using characteristic mode analysis. *IEEE Transactions on Antennas and Propagation* **66**(4), 1894–1902.
13. **Liang Z, Ouyang J and Yang F** (2018) Design and characteristic mode analysis of a low-profile wideband patch antenna using metasurface. *Journal of Electromagnetic Waves and Applications* **32**(17), 2304–2313.
14. **Sun Y, Meng W and Xu J** (2022) High-gain and wideband differentially fed circularly polarized planar aperture antenna. *Microwave and Optical Technology Letters* **64**, 2059–2066.
15. **Wu R, Liao K and Dong J** (2022) Polarization conversion metasurface antenna based on characteristic mode analysis. In *2022 IEEE MTT-S International Wireless Symposium (IWS)*, Harbin, China, 1–3.
16. **El Yousfi A, Lamkaddem A, Abdalmalak KA and Segovia-Vargas D** (2023) A broadband circularly polarized single-layer metasurface antenna using characteristic-mode analysis. *IEEE Transactions on Antennas and Propagation* **71**(4), 3114–3122.
17. **Ding Z, Xu M, Li X, Tao S, Wang H and Wang Y** (2023) Design of wideband circularly polarized metasurface antenna using characteristic mode analysis. *Microwave and Optical Technology Letters* **65**, 1794–1799.
18. **Gao G, Meng H, Geng W, Zhang B, Dou Z and Hu B** (2021) Design of a wide bandwidth and high gain wearable antenna based on nonuniform metasurface. *Microwave and Optical Technology Letters* **63**, 2606–2613.

https://doi.org/10.1017/S1759078724000588 Published online by Cambridge University Press

19. **de Dieu Ntawangaheza J, Sun L, Wang S, Li Y, Zheng Z, Biao D and Rushingabigwi G** (2021) A single-layer low-profile broadband metasurface-inspired antenna with monopole-like radiation characteristics. *IEEE Transactions on Antennas and Propagation* **70**(6), 4818–4823.

Hui Pang was born in Weifang, China, in 1999. She received the B.E. degree in software engineering from Qufu Normal University, Qufu, China, in 2021. She is currently pursuing the M.E. degree with Qufu Normal University. Her current research interests include metamaterials based antenna and microstrip antenna.

Jianping Zhao is a professor and supervisor of master students. In 1981, he entered the Physics Department of Qufu Normal University, and in 1988, he pursued a master's degree in Radio and Information Engineering at Wuhan University. His current research interests include wireless communication technology and design of electronic technology applications.

Juan Xu was born in 1982 and graduated from Nanjing University of Science and Technology in 2016 with a Ph.D. in electronic science and technology. She is currently an associate professor of Cyber Science and Engineering, Qufu Normal University. Her research interests mainly include microwave/millimeter wave circuits and systems, integrated circuit, antenna array optimization and beam forming, multifunctional electromagnetic metasurface, and terahertz biosensing.

https://doi.org/10.1017/S1759078724000588 Published online by Cambridge University Press